Experimental investigation of two-side heat transfer in spacer-filled channels

Experimental investigation of two-side heat transfer in spacer-filled channels

M Ciofalo, F Cacciatore, M Di Liberto and A Tamburini

Dipartimento di Ingegneria, Università degli Studi di Palermo, viale delle Scienze Ed. 6, 90128 Palermo, Italy
Corresponding author e-mail: michele.ciofalo@unipa.it

Abstract. In Membrane Distillation (MD), spacers support the membranes and promote mixing, thus reducing temperature polarization. Their efficient design requires a knowledge of the distribution of the local heat transfer coefficient *h* and of its dependence on Reynolds number, spacer geometry and flow-spacer relative orientation. In previous work, we applied Thermochromic Liquid Crystals (TLC) and digital image processing to the measurement of *h* distributions for different spacer configurations; data were used to validate CFD simulations and select turbulence models. For constructive reasons, the test section allowed only one-side heat transfer, while in most MD configurations (e.g. spiral-wound modules) heat transfer occurs from both sides of the feed water channels. Analytical and numerical solutions show that changing from one-side to two-side heat transfer deeply affects *h* values. This motivated the design and construction of an improved test section in which a hot channel is sandwiched between two cold channels, and twin cameras and lighting equipment allow the simultaneous acquisition of TLC images on both walls. This paper describes this new test section and the experimental technique, discusses measurement uncertainty, and presents preliminary results.

1. Introduction

Membrane distillation (MD) is a separation technique combining the features of thermal and membrane processes [1]. Thermal energy causes the liquid to vaporise in an evaporator channel, while a hydrophobic micro-porous membrane allows the passage of vapour only to a condenser channel (figure 1).

Although other applications are possible, here we focus on MD as a means to produce drinkable water from saline water. In this field, MD is currently being investigated worldwide as a low cost, energy saving alternative to thermal distillation and reverse osmosis. Since it operates at temperatures well below saturation, it can be powered by solar energy and waste heat [2, 3].

In MD, the driving force is the temperature difference between feed and permeate (typically 5 to 50 K). The feed channel thickness usually ranges from 2 to 5 mm and the flow velocity from 5 to 20 cm/s, yielding Reynolds numbers from 200 to 2000.

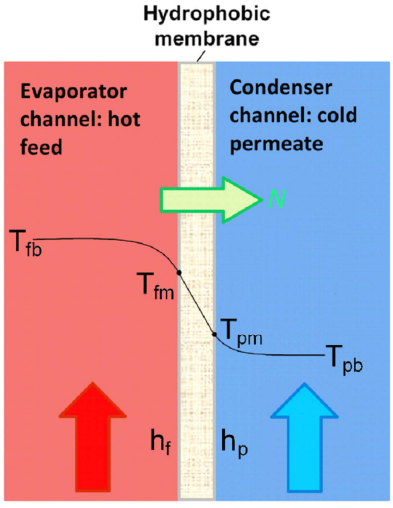

Figure 1. MD principle

The finite values of heat and mass transfer coefficients cause polarization phenomena, of which temperature polarization in the feed channels is the most important [4]. With reference to figure 1, polarization reduces the driving force of the process from the maximum possible one, T_{fb}-T_{pb}, to the lower value T_{fm}-T_{pm} (subscripts "*f*" and "*p*" refer to feed and permeate while "*m*" and "*b*" refer to membrane surface and fluid bulk, respectively). Polarization decreases with the Reynolds number, especially for low Re, and increases with the heat flux. Therefore, as improved membranes for MD are

being developed, temperature polarization may become the dominant factor limiting flux enhancement, thus hindering the above efforts.

The main solution proposed to the problem of temperature polarization is the enhancement of mixing in the feed channels. This is usually accomplished by means of spacers, normally interposed between consecutive membrane sheets in planar or spiral-wound modules to mechanically support the membranes [5]. Spacers have the undesirable effect of increasing pressure drop, but this is usually a minor issue in MD, where the pumping cost is only a small fraction of the overall cost.

The spacers adopted in MD applications (figure 2) are usually nets consisting of two or more layers of polymeric wires, often designed and commercialized for different applications. Their effectiveness, as quantified by the local heat transfer coefficient h distribution and by its surface-averaged value $\langle h \rangle$, has been the subject of several experimental [6, 7] and computational [8, 9] efforts.

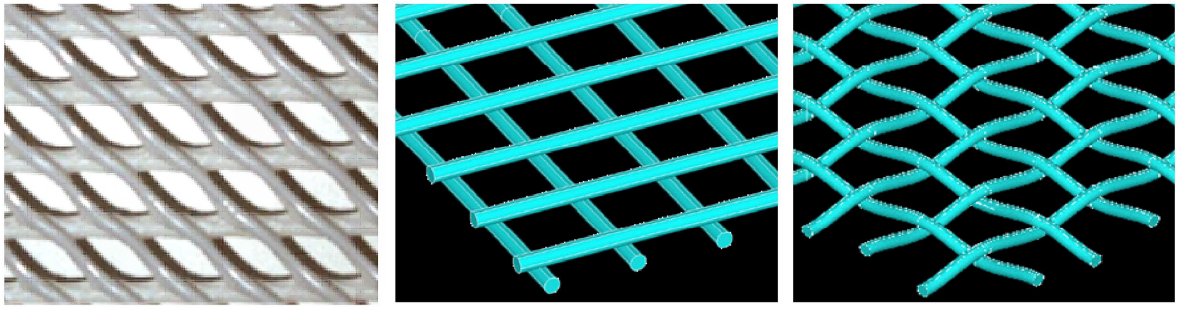

(a) (b) (c)

Figure 2. Some spacer types: (a) extruded; (b) overlapped; (c) woven

2. Previous work

In this Department a suite of test sections were built and used to study heat transfer in channels filled with different types of spacers under conditions representative of MD. Wall temperatures were measured by Thermochromic Liquid Crystals (TLC), whose use is well documented in the scientific literature both for the measurement of surface temperature distributions [10] or for the joint visualization of flow and temperature fields [11]. Details of the experimental procedure were described in previous papers [12, 13], and only a short description will be provided here.

The test sections consisted of a hot and a cold channel separated by a 1 mm thick transparent polycarbonate (PC) layer and closed by Plexiglas® slabs. Hot water was forced to flow through one of the channels, filled with the spacer to be tested whose thickness established the channel height H. A sheet of Hallcrest® thermochromic liquid crystals, ~0.12 mm thick, was interposed between the spacer and the polycarbonate layer, with its visible surface touching this latter; a thin layer of transparent silicone grease was used to provide adhesion and thermal contact between the TLC sheet and the PC layer. Cold water was forced in parallel flow on the opposite side of the polycarbonate layer, i.e. within the cold channel, which was left void and whose height was 3 mm. In a first stage [12] commercial MD spacers, typically 3-4 mm thick, were tested, but in subsequent work [13] a scaled-up configuration was preferred, using purpose manufactured spacers and characterized by H=1 cm.

In order to define dimensionless quantities, reference was made to the corresponding "void" configuration, i.e. to a spacerless, laterally indefinite, plane channel of height H and hydraulic diameter $2H$. Thus, the definition of the bulk Reynolds number was

$$\mathrm{Re} = \frac{U \cdot 2H}{\nu} = \frac{2Q}{W \cdot \nu} \tag{1}$$

$U = Q/(WH)$ being the mean "void channel" streamwise velocity (superficial velocity), Q the volume flow rate and W the channel's lateral dimension. This scaling is preferable to one based, for each specific geometry, on the actual hydraulic diameter and mean velocity (interstitial velocity), because it better highlights the influence of a given spacer configuration [14].

The TLC colour distribution was recorded by a digital camera through the outer Plexiglas® wall of the cold channel, the cold water, the polycarbonate layer, and the transparent polyester foil which makes up most of the TLC sheet's thickness. Images were split into HSV (Hue, Saturation, Value) components; Hue was converted into temperature on the basis of an *in-situ* calibration.

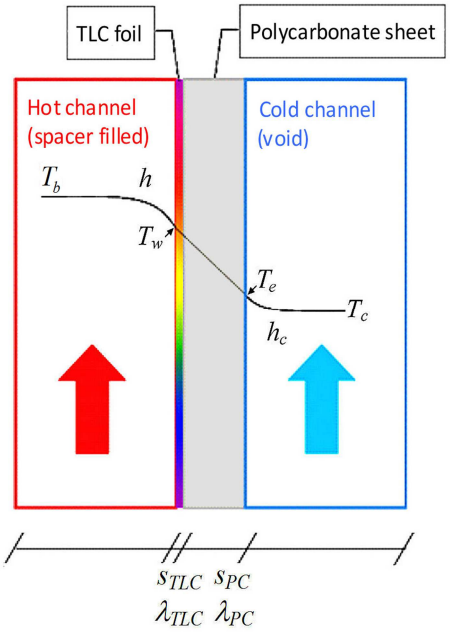

The temperature profile across the different layers on a side of the test section is schematically shown in figure 3. The close analogy with figure 1 should be observed. An analysis of the heat transfer process under the assumption of one-dimensional transport gives the local hot-side heat transfer coefficient h as a function of the locally measured temperature T_w of the TLC sheet once the bulk temperatures T_b, T_c of the hot and cold fluids and the cold-side heat transfer coefficient h_c are known:

$$h = \left[\frac{s_{TLC}}{\lambda_{TLC}} + \frac{s_{PC}}{\lambda_{PC}} + \frac{1}{h_c} \right]^{-1} \cdot \frac{T_w - T_c}{T_b - T_w} \qquad (2)$$

The term in square brackets is an overall thermal resistance r, made up of the conductive thermal resistances s/λ of the thermochromic liquid crystal film (*TLC*) and of the polycarbonate layer (*PC*), in series with the cold-side convective thermal resistance $1/h_c$.

Figure 3. Temperature across the test section.

T_b and T_c were measured by Pt100 RTDs at the inlet and outlet of the hot and cold channels and their linear variation along the flow direction was assumed. The coefficient h_c was estimated by the Dittus-Bölter correlation ($Nu=0.023\ Re^{0.8}\ Pr^{0.4}$) applied to the turbulent flow in the cold channel.

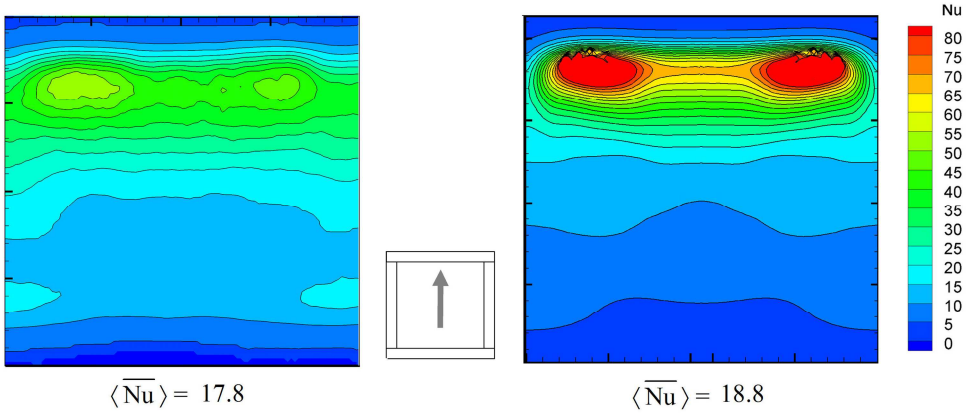

Figure 4. Single-side heat transfer: experimental (left) versus DNS (right) distributions of the local Nusselt number on the top wall for P/H=2, Re≈600 and a flow attack angle θ=90°. The inset shows the flow direction and the spacer wire arrangement. Adapted from [13].

As an example of the results obtained, figure 4 (left) shows experimental distributions of the local Nusselt number Nu on the thermally active wall of a unit cell for an overlapped spacer having pitch to height ratio P/H=2 and a flow attack angle of 90°. The map is an average over 6 adjacent unit cells and 10 consecutive time instants. The map on the right is the corresponding time-averaged distribution predicted by Direct Numerical Simulation (DNS). The inset shows the flow direction in relation with

the arrangement of the spacer wires. Average values of Nu are also reported.

The main features of the Nu distributions are fairly well predicted by the numerical simulations. DNS overestimates peak values of Nu, but average values ⟨Nu⟩ are only slightly overpredicted. The agreement between experimental and DNS results can be regarded as a mutual validation of the results, since in the simulations the continuity, Navier-Stokes and enthalpy transport equations are directly solved, no turbulence model is used and the experimental conditions are faithfully reproduced.

3. One-side versus two-side heat transfer

A fluid-filled channel can be subjected to different types of heat transfer on the two sides. In Membrane Distillation, one-side heat transfer is usually realized in laboratory-scale experimental rigs [4, 12, 13] or small-scale, plate-and-frame, MD equipment [15, 16] because it is simpler to build and allows an easier measurement of temperatures and heat fluxes. Commercial MD plants usually exhibit heat and mass transfer from both sides of the feed channels. An example are the spiral wound modules developed at the Fraunhofer Institute [17] and shown in figure 5: the hot (feed) channel is placed between two membranes followed by two condensate channels, two conductive walls and two cooling channels, and the whole arrangement is spirally wound to achieve compactness and reduce heat losses.

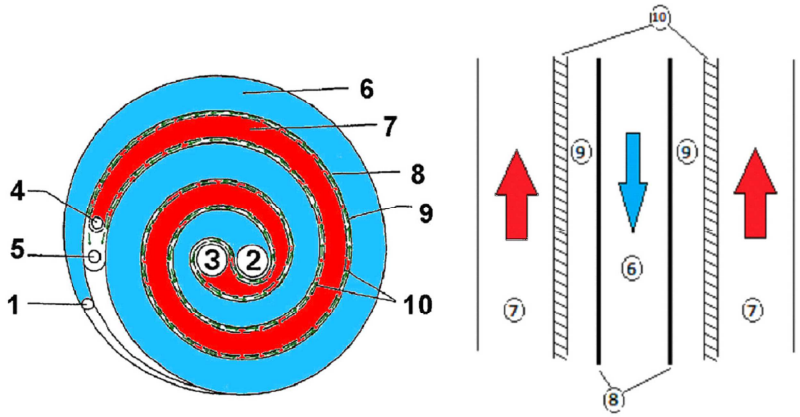

(a) (b)

Figure 5. Sketch of a Fraunhofer spirally wound MD module (adapted from [17]). (a) Transverse section, showing (1) coolant inlet; (2) coolant outlet; (3) feed inlet, (4) feed outlet; (5) condensate outlet; (6) coolant; (7) feed; (8)-(9) membranes, (10) condensate channels. (b) Longitudinal section, showing (6) coolant, (7) feed, (8) dividing foils, (9) condensate channels, (10) membranes.

For channels filled with overlapped spacers having a pitch-to-height ratio P/H=2, figure 6 (obtained by CFD for steady laminar flow) compares the mean Nusselt numbers on both walls in two-side heat transfer with the mean Nusselt number on the single active (top) wall in one-side heat transfer for θ=0° (a) or θ=45° (b). For θ=0° (main flow aligned with the spacer filaments adjacent to the top wall), graph (a), the mean Nusselt number for one-side heat transfer from the top wall exhibits a completely different behavior than the top, bottom or average ⟨Nu⟩ obtained for two-side heat transfer; in particular, it is considerably larger for Re<~200 but becomes smaller for larger Re.

For the flow attack angle of 45°, graph (b), ⟨Nu⟩ values on the two walls in two-side heat transfer are identical for symmetry reasons. The trends of the two-side and one-side curves are similar, but the two-side mean Nusselt number is 20-30% larger than its one-side counterpart at all Re, so that the overall thermal power exchanged for any bulk to wall temperature difference is from 2.4 to 2.6 times larger (of course, the heat transferred *per unit membrane area* is only 1.2~1.3 times larger).

From these results it can be concluded that experimental and computational results obtained for one-side transfer cannot be extended to two-side transfer, because not only the absolute values of the surface-averaged Nusselt numbers, but also their trends with Re and other parameters, may differ significantly, so that the performance ranking of the various configurations examined may be altered.

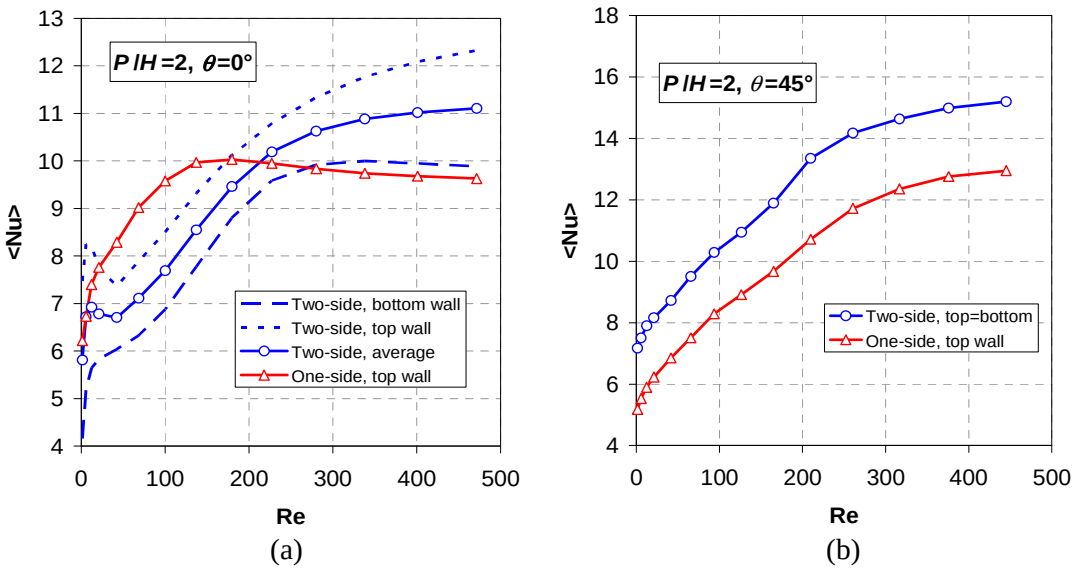

Figure 6. One-side vs. two-side heat transfer for overlapped spacers with P/H=2. Mean values of Nu on the top and bottom walls and their average in two-side heat transfer are reported as functions of the Reynolds number, along with the mean values of Nu on the only active wall (top wall) in one-side heat transfer. (a) θ=0°; (b) θ=45°. In this latter case one has $\langle Nu \rangle_{top} = \langle Nu \rangle_{bottom}$. Adapted from [18].

4. New test section

The above considerations on the difference between one-side and two-side heat transfer were the main motivation for building a new test section allowing the latter condition to be achieved.

Figure 7 highlights the main difference between the new test section and the previous ones [12, 13] by comparing the respective cross sections. In the new equipment, the hot water channel is sandwiched between two cold water channels in a geometrically and thermally symmetric arrangement and in parallel flow.

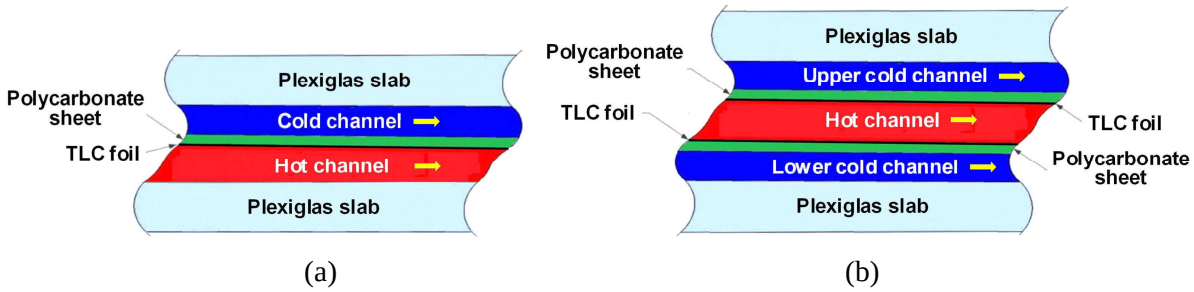

Figure 7. Cross sections of the previous test sections (a) and of the new test section (b).

The presence of two-side heat transfer made a deep re-design of the whole test section necessary. The need for allowing the inflow and outflow of three separate streams, in particular, was particularly demanding. The design solution adopted is sketched in the exploded view of figure 8, which shows the different layers and the path of the fluids.

Top and bottom walls consist of 30 mm thick Plexiglas® slabs, each bearing three slots for the passage of hot and cold water. Suitably shaped rubber gaskets, 3 mm thick, delimit the upper and lower cold water channels. A third, thicker (10 mm) rubber gasket delimits the hot water channel and surrounds the spacer.

The test section is provided with suitable fittings and inflow-outflow manifolds and is kept closed by stiff stainless steel profiles with the help of bolts which are tightened by a dynamometric wrench. On each side of the test section, a suitable steel structure holds a Canon EOS® 24 Mpixel camera and two 100 W halogen bulbs, powered through a continuity group to ensure a constant supply voltage.

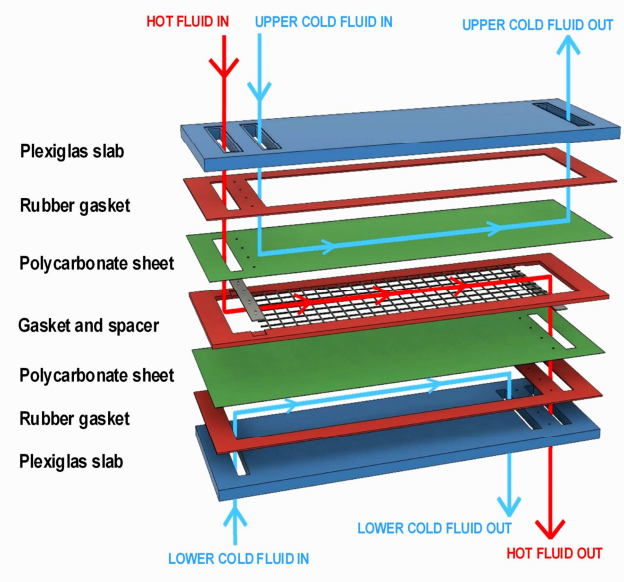

Figure 8. Exploded view of the new test section, showing the various layers and the fluids paths

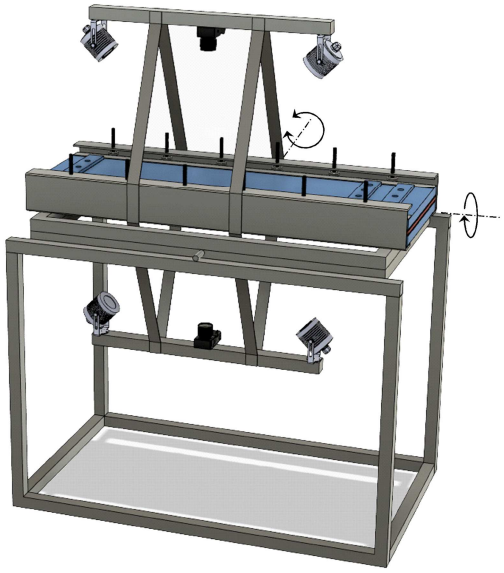

Figure 9. Test section and photographic equipment on their tilting support.

The whole assembly is fixed to a tilting support which can rotate around two orthogonal directions to facilitate filling-voiding and the removal of air bubbles (figure 9).

Hot water is provided by a Julabo® ED-5 thermo-static bath, while cold water is drawn from a 100 L tank cooled by a Corema® Junior Chiller JA/C 150 with the interposition of a copper coil. Distilled water is used through all tests to reduce scaling. Hot and cold water flow rates are measured by two Krone® Optiflux-5300 magnetic flow meters.

Inlet and outlet temperatures of the three fluid streams (one hot, two cold) are measured by six PT100 RTDs and are acquired on a PC by a National Instruments® data acquisition systems; temperature data are taken every 0.1 s and averaged over 60 or 120 s to reduce random fluctuations. Pressure tappings are placed in the hot channel, about 40 cm apart, and the pressure drop is measured by a Fuji Electric® FKC-33 differential manometer.

Inlet and outlet pressures are also approximately measured by six standpipe piezometers, ~4 m in height, which also serve as pressure limiters. Inlet, outlet and bypass valves can be adjusted to provide the required flow rates while maintaining a slightly higher pressure (e.g. 1 m water column) in the cold channels than in the hot channel, so that the polycarbonate sheets are kept tightly pressed against the spacer. By suitably regulating the valves, it is also possible to send water from the thermo-static bath to all three channels (configuration used for the TLC calibration) or to keep one of the cold channels empty (configuration providing a practically adiabatic wall and thus one-side heat transfer conditions).

5. Preliminary results and remarks on uncertainty

As an example of the potentiality of the method and of the test section described above, figure 10 reports results obtained for P/H=4, θ=0° (top wall) or 90° (bottom wall), and a hot fluid flow rate of 316 L/h, yielding a Reynolds number of ~780. For this test case, linear interpolation of the inlet and outlet PT100 readings provided for the local hot fluid bulk temperature a value of 32.06°C in the region of interest. Similarly, the cold fluid bulk temperatures were estimated to be 21.72°C (top) and 21.67°C (bottom).

Graphs (a) and (b) are unprocessed pictures of a small portion of the TLC-covered top and bottom walls, respectively. Graphs (c) and (d) are corresponding maps of the wall temperature distributions, obtained from the *Hue* component of the images by *in situ* calibration. Finally, graphs (e) and (f) are maps of the local hot-side heat transfer coefficient h, estimated by Eqs. (2)-(3).

Note that both the photographs and the maps obtained by their post-processing are instantaneous and local, and thus are affected by the turbulent fluctuations already present in this geometry at the

Reynolds number considered (780). More regular results would be obtained by applying to the instantaneous and local distributions either time averaging (over several consecutive frames), or *ensemble* averaging (over several adjacent, and ideally equivalent, unit cells), or both, as was done, for example, in the single-side heat transfer test cases illustrated in Figure 4.

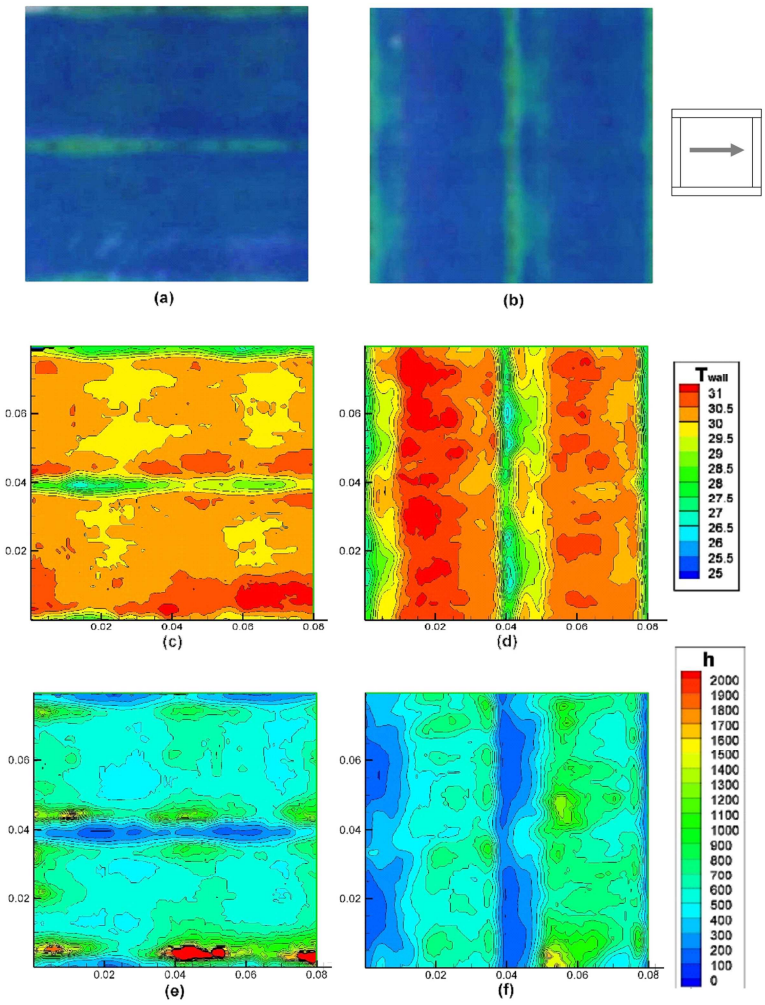

Figure 10. Results obtained for Re=780, P/H=4, θ=0° (top) or 90° (bottom). (a), (b): photographs of 2×2 cell regions of the TLC-covered top and bottom walls, respectively; (c), (d): corresponding wall temperature distributions; (e), (f): corresponding hot-side wall heat transfer coefficient distributions.

Uncertainty analysis is based on the theory of error propagation and is essentially the same as for the case of single-side heat transfer [12, 13]. Under typical test conditions, the *relative* uncertainty σ_h/h is proportional to the local value of h and varies between ~10% and ~15% over most of the unit cell, with higher values (up to ~20%) only in correspondence with h maxima. A larger relative uncertainty exists in the areas where the active wall touches the spacers, but here h is very low so that the absolute uncertainty on h is negligible. Although a relative uncertainty of 10 to 20% may look large, the advantage of a high spatial resolution, whole-field assessment of h is priceless, especially if the influence of the spacer geometry and flow attack angle have to be investigated with a view to develop higher-performance spacers.

6. Conclusions

The new test section described in the present paper allowed the simultaneous measurement of the local heat transfer coefficient h on both walls of spacer-filled plane channels cooled from two sides. With

respect to previous studies, this configuration is more closely representative of the conditions holding in a real Membrane Distillation module. Preliminary tests yielded satisfactory results, although *h* was affected by considerable uncertainties. Work is currently in progress to improve the results by optimizing the cold channel thickness and flow rate, applying time- and ensemble-averaging techniques and replacing the one-dimensional heat flux assumption underlying equation (1) by a more accurate inverse heat conduction algorithm.

References

[1] Lawson K W and Lloyd D R 1997 Membrane distillation *J. Membr. Sci.* **124** 1–25.
[2] Schwantes R, Cipollina A, Gross F, Koschikowski J, Pfeifle D, Rolletschek M and Subiela V 2013 Membrane Distillation: solar and waste heat driven demonstration plants for desalination *Desalination* **323** 93-106
[3] Chiavazzo E, Morciano M, Viglino F, Fasano M and Asinari P 2018 Passive solar high-yield seawater desalination by modular and low-cost distillation *Nature Sustainability* **1** 763-772
[4] Ali A, Macedonio F, Drioli E, Aljlil S and Alharbi O A 2013 Experimental and theoretical evaluation of temperature polarization phenomenon in direct contact membrane distillation *Chem. Eng. Res. Des.* **91** 1966–1977
[5] Martínez-Díez L, Vázquez-González M I and Florido-Díaz F J 1998 Study of membrane distillation using channel spacers *J. Membr. Sci.* **144** 45-56
[6] Chernyshov M N, Meindersma G W and de Haan A B 2005 Comparison of spacers for temperature polarization reduction in air gap membrane distillation *Desalination* **183** 363-74
[7] Yun Y, Wang J, Ma R and Fane A G 2011 Effects of channel spacers on direct contact membrane distillation *Desalination and Water Treatment* **34** 63-69
[8] Koutsou C P, Yiantsios S G and Karabelas A J 2007 Direct numerical simulation of flow in spacer-filled channels: effect of spacer geometrical characteristics *J. Membr. Sci.* **291** 53–69
[9] Shakaib M, Hasani S M F, Ahmed I and Yunus R M 2012 A CFD study on the effect of spacer orientation on temperature polarization in Membrane Distillation modules *Desalination* **284** 332–340
[10] Stasiek J A, Collins M W, Ciofalo M and Chew P E 1996 Investigation of Flow and Heat Transfer in Corrugated Passages–I.Experimental Results *Int. J. Heat Mass Transf.* **39** 149-64
[11] Ciofalo M, Signorino M and Simiano M 2003 Tomographic particle-image velocimetry and thermography in Rayleigh-Bénard convection using suspended Thermochromic Liquid Crystals and digital image processing *Experiments in Fluids* **34** 156-72
[12] Tamburini A, Pitò P, Cipollina A, Micale G and Ciofalo M 2013 A Thermochromic Liquid Crystals Image Analysis technique to investigate temperature polarization in spacer-filled channels for membrane distillation *J. Membr. Sci.* **447** 260-73
[13] Tamburini A, Renda M, Cipollina A, Micale G and Ciofalo M 2016 Investigation of heat transfer in spacer-filled channels by experiments and direct numerical simulations *Int. J. Heat Mass Transf.* **93** 1190-205
[14] La Cerva M, Ciofalo M, Gurreri L, Tamburini A, Cipollina A, Micale G 2017 On some issues in the computational modelling of spacer-filled channels for membrane distillation *Desalination* **411** 101-111
[15] Cipollina A, Di Sparti M G, Tamburini A and Micale G 2012 Development of a Membrane Distillation module for solar energy seawater desalination *Chem. Eng. Res. and Des.* **90** 2101–21
[16] Francis L, Ghaffour N, Alsaadi A S, Nunes S P and Amy G L 2014 Performance evaluation of the DCMD desalination process under bench scale and large scale module operating conditions *J. Membr. Sci.* **455** 103–12
[17] Winter D, Koschikowski J and Wieghaus M 2011 Desalination using membrane distillation: experimental studies on full scale spiral wound modules *J. Membr. Sci.* **375** 104–12
[18] Ciofalo M, La Cerva M, Di Liberto M and Tamburini A 2017 Influence of the boundary conditions on heat or mass transfer in complex channels *J. Phys. – Conf. Ser.* **923** 012053